A computational approach to fretting wear prediction at the head-stem taper junction of total hip replacements

Russell English, Ariyan Ashkanfar* and Glynn Rothwell

School of Engineering, Technology and Maritime Operations, Liverpool John Moores University, Byrom Street, Liverpool, L3 3AF, UK

Abstract

Wear is one of the main reasons for failure of modular total hip replacements. Recent evidence suggests that fretting wear occurs at the taper junction which provides fixation between the prosthesis femoral head and stem components. The fine metallic wear debris that is released can lead to adverse soft-tissue reactions which can necessitate a revision surgery. The present study proposes a computational methodology utilising an energy wear law and a 3D finite element model to predict fretting wear at the taper junction. The method is novel in that it simulates the weakening of the initial taper 'fixation' (created at impaction of the head onto the stem in surgery) due to the wearing process. The taper fixation is modelled using a contact analysis with overlapped meshes at the taper junction. The reduction in fixation is modelled by progressive removal of the overlap between components based on calculated wear. The fretting wear analysis approach has been shown to model the evolution of wear effectively; however, it has been shown that accurate, quantitative values for wear are critically dependant on mesh refinement, wear scaling factor and fraction, wear coefficient used and knowledge of the device loading history. The method has been implemented with a 3D finite element model of the taper junction of a commercial total hip replacement. This has been used to determine taper wear patterns, wear damage and wear rates which have been shown to be consistant with those found from observation and measurement of retrieved prostheses. The numerical method could be used to consider the effect of design changes and clinical technique on subsequent fretting wear in modular prosthetic devices.

Keywords: Wear modelling; Finite element modelling; Fretting; Hip joint prosthesis; Total hip replacements; Taper junction.

* Corresponding author. Tel: +44 151 231 2028, +44 759 198 0781. E-mail address: a.ashkanfar@2012.ljmu.ac.uk, ariyan.ashkanfar@gmail.com (A. Ashkanfar).

1. Introduction

A hip joint can allow a wide range of movement and transmit high dynamic loads. Its performance to carry loads and provide this mobility is remarkable; however, it is vulnerable and can lose its functionality due to disease such as osteoarthritis or bone fracture. At the final stage of severe hip pathologies, arthroplasty is a key solution for patients who wish to pursue an active lifestyle again.

Modular Total Hip Replacements (THRs) (Fig. 1) allow a surgeon to choose different prosthesis components for individual patients dependent on their anatomy, age and level of activity. The prosthetic femoral head in THR is assembled to the stem using a conical taper fixation. The head is impacted onto the stem trunnion intraoperatively with long-term and safe fixation of the assembly dependent on the taper junction design and the impaction load applied [1].

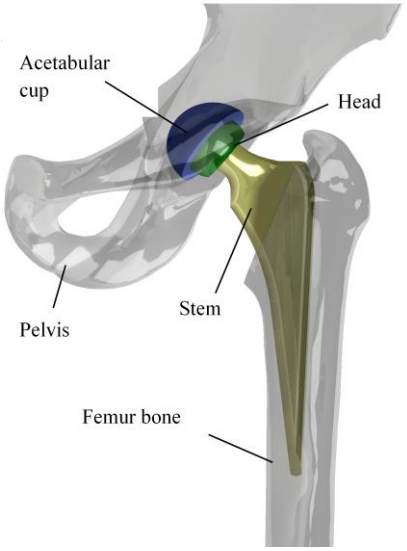

Fig. 1. Schematic of total hip replacement *in situ.*

Recent data from the National Joint Registry (NJR) indicates that around 89,000 hip operations were performed in the UK using arthroplasty in 2013 (11th Annual Report 2014, NJR for England, Wales and Northern Ireland, 2014). The American Academy of Orthopaedic Surgeons (AAOS) has indicated that more than 285,000 THRs are performed each year in the United States (National Hospital Discharge Survey, USA, 2010). Instances of premature failure of these implants (<5 years) has been reported and attributed to aseptic loosening [2, 3]. In addition, a significant increase in the number of young active patients requiring hip prostheses has led to much research to increase the operating life of these devices. Thus, one of the main mechanical requirements for an improved prosthetic design is to minimise wear in order to increase device longevity.

The wear debris produced from these devices is created at the acetabular cup and head articulating surface, and also from the head-stem taper junction [2]. Many studies have been published on determining wear in prosthetic devices which have mainly focused on the articulating surfaces between the head and acetabular (plastic) cup [4-11]. Modern large diameter Metal-on-Metal (MoM) THRs were introduced around 1997 [12] as an option for young active patients to provide a device with reduced wear debris and risk of dislocation, greater strength and longer life than Metal-on-Plastic (MoP) types. However, under certain circumstances, metal debris can be generated at the articulating surfaces which can damage the surrounding soft tissues and cause immobility in patients [13]. Importantly, evidence of metal wear debris has been reported in MoP (case-report level) and Ceramic-on-Ceramic (CoC) THRs too implicating taper wear and also neck-cup impingement [2, 14]. Langton, et al. [15] and Bolland, et al. [16] have shown damage at the taper junction in retrieved MoM prostheses where there is correspondingly minimal wear at the bearing surfaces but still serious soft tissue damage. Langton, et al. [15] presented Scanning Electron Microscope (SEM) images of taper junction surface damage occurring in the femoral heads from retrieved large diameter MoM THRs. The images show surface peaks (created by the impression of the machining grooves from the trunnion) having been sheared off leading to significant material loss, and evidence of the formation of pits with inclusions which it was hypothesised were primarily due to mechanical fretting wear. There was evidence of only small amounts of chlorides and oxides suggesting corrosion was not the primary mechanism of material loss, contrary to the opinion of Malviya, et al. [17], Goldberg, et al. [18], and Gilbert, et al. [19]. There is evidence in the literature of experimental investigations relating to fretting in THRs [20, 21] but only a limited number of studies on the numerical simulation of this type of wear [22, 23]. It is apparent that further research is required to help inhibit the effects of corrosion; however, the work presented here focuses solely on fretting wear as being the primary mechanism causing damage at the head-stem taper junction in THRs.

A computational method is presented to predict fretting wear at the head-stem taper junction which can be used in addition to testing [22-26] to help improve the wear characteristics of prosthesis designs. The method is unique in that it models the progressive weakening of the taper ‘fixation’ due to the fretting wear process. This ‘reduction’ in fixation is modelled using a static contact analysis incorporating mesh overlap at the taper interface. As wear occurs at the interface over time the overlap is removed accordingly

by updating the contacting nodes positional coordinates. A three dimensional finite element model of a commercial THR is used to demonstrate the method and to highlight key features of the wear algorithm. The wear damage, depth, rate and patterns of wear are shown to be comparable with those found in the literature and from observation from available retrieved prostheses. The model could be used to identify key factors leading to debris release at the taper junction so that appropriate prosthesis design and surgical procedural modifications can be made to mitigate against this damaging problem.

2. Wear

The methodology described here allows for the implementation of either the 'Archard' or the 'Dissipated Energy' wear law for the prediction of fretting wear. However, the energy wear approach is presented here as a single energy wear coefficient unifies prediction of wear across a wider range of stroke (50 μm to 1.3 mm) than Archard and as such has a greater range of application [27-29].

2.1 Wear law and FE implementation

The energy wear law Eq. (1) bases the calculation of volumetric wear on the interfacial shear work being the predominant parameter determining wear. It shows that the total volumetric wear W_v is obtained from the product of the total local accumulated dissipated energy E and an energy wear coefficient α:

$$W_v = \alpha E \tag{1}$$

where

$$E = Qs \tag{2}$$

and Q is the shear traction and s the relative displacement between the contacting surfaces, giving:

$$W_v = \alpha Q s \tag{3}$$

By dividing both sides of Eq. (3) by a contact area, the linear wear depth W_d can be calculated using Eq. (4), where τ is the contact surface shear stress:

$$W_d = \alpha \tau s \tag{4}$$

For the numerical implementation of this wear law, the process used here is to first determine the wear depth at contacting surfaces generated by a single loading cycle on the components (such as the *in-vivo* loading applied on a hip for a single walking step); subsequently, as the components will typically be

subject to millions of loading cycles during their lifetime, this single cycle wear depth is multiplied by a 'wear scaling factor β' so as to make the execution of an analysis achievable in an acceptable period of time. The 'wear scaling factor' represents a specific number of loading cycles (e.g., 10^5) and its value depends on how accurately the evolution of wear is to be calculated, with a trade off against time. After scaling the wear depth, the geometry of the contacting surfaces of the components are then modified to reflect the wear that would have occurred over the period of β cycles. The calculated wear can be applied to one component only, or to both in either equal or unequal amounts dependant on the material combinations in contact. The process is then repeated using the updated geometry until a specified number of cycles of loading have been applied or a pre-specified wear depth has been reached.

In order to model accurately the effect on wear of a time-variant load distribution during a loading cycle (such as occurs during walking) it is necessary to discretise the loading cycle into a number of time intervals n. As such, the wear depth for a single cycle of loading (the cyclic wear depth W_c) can be calculated using Eq. (5), where τ_i and s_i are respectively the surface shear stress and relative displacement calculated at the end of a specific time interval i.

$$W_c = \sum_{i=1}^{n} \alpha \tau_i s_i \tag{5}$$

The total wear depth W_d that is generated over a specified total number of loading cycles N can be determined from Eq. (6), where j represents a specific 'analysis stage' reflecting the evolution of wear:

$$W_c = \sum_{j=1}^{(N/\beta)} \beta \sum_{i=1}^{n} \alpha \tau_i s_i \tag{6}$$

The accuracy and efficiency of this approach is dependent on numerous factors, not least of which is the magnitude of the energy wear coefficient α used. In addition, the number of intervals i used to discretise the loading cycle, and the magnitude of the 'wear scaling factor β need careful consideration in terms of their influence on accuracy and analysis run times.

The energy wear law in the form of Eq. (6) can be used in conjunction with the FE method to calculate wear depth at the contacting surfaces of an FE model. The calculation of relative displacement at the contact interface is facilitated by creating sets of 'paired nodes' at the contacting surfaces (Fig. 2). This 'pairing' is achieved by determining which nodes on opposite mating surfaces are closest to each other

geometrically prior to loading (at the start of the analysis and at the start of a new analysis 'stage' following a geometry update).

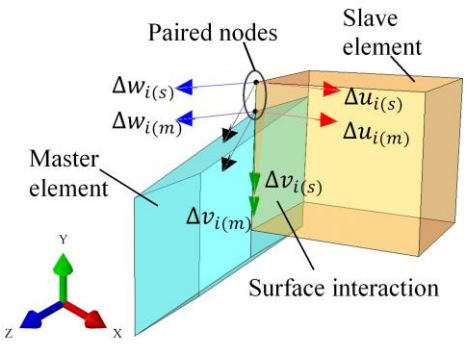

Fig. 2. Nodal pairing and calculation of relative displacement.

The surface shear stress and displacements of all nodes which have been paired are extracted from the FE analysis at the end of each loading time interval i. These extracted values are then processed to provide values for use in the calculation of the cyclic wear depth.

As the paired nodes may not be exactly coincident (before and after loading) an average value of shear stress τ_{ip} is calculated for each nodal pairing as defined by Eq. (7), where τ_{master} and τ_{slave} are the surface shear stresses on the master and slave surface respectively for each set of paired nodes.

$$\tau_{ip} = \frac{|\tau_{master}| + |\tau_{slave}|}{2} \tag{7}$$

For the 3D FE model, the relative displacement between paired nodes s_{ip} which has occurred during a time interval is calculated from the displacements of both the master and slave nodes in a pair at the end of the time interval i (see Fig. 2). Specifically, for each set of paired nodes, s_{ip} is calculated from Eq. (8),

$$s_{ip} = \sqrt{s_{ix}^2 + s_{iy}^2 + s_{iz}^2} \tag{8}$$

where s_{ix} , s_{iy} and s_{iz} are the Cartesian component relative displacements of the paired nodes in the x, y and z directions respectively, they can be determined from Eq. (9),

$$\begin{aligned} s_{ix} &= \Delta u_{i(m)} - \Delta u_{i(s)} \\ s_{iy} &= \Delta v_{i(m)} - \Delta v_{i(s)} \\ s_{iz} &= \Delta w_{i(m)} - \Delta w_{i(s)} \end{aligned} \tag{9}$$

where $\Delta u_{i(m)}$, $\Delta u_{i(s)}$ are the nodal displacements that have occurred during time interval i in the x-direction for the paired master and slave nodes respectively, with $\Delta v_{i(m)}$, $\Delta v_{i(s)}$ and $\Delta w_{i(m)}$, $\Delta w_{i(s)}$ being the

corresponding displacements in the y and z-directions (Fig. 2). The nodal displacements in an interval are calculated using Eq. (10) and are the difference in the total nodal displacement values u, v and w at the end of a time interval i+1 and the start i.

$$\begin{aligned}
\Delta u_{i(m)} &= u_{i+1(m)} - u_{i(m)} \\
\Delta u_{i(s)} &= u_{i+1(s)} - u_{i(s)} \\
\Delta v_{i(m)} &= v_{i+1(m)} - v_{i(m)} \\
\Delta v_{i(s)} &= v_{i+1(s)} - v_{i(s)} \\
\Delta w_{i(m)} &= w_{i+1(m)} - w_{i(m)} \\
\Delta w_{i(s)} &= w_{i+1(s)} - w_{i(s)}
\end{aligned} \tag{10}$$

The total wear depth at the point locations of the paired nodes W_{dp} is found from Eq. (11),

$$W_{dp} = \sum_{j=1}^{(N/\beta)} \beta \sum_{i=1}^{n} \alpha \tau_{ip} s_{ip} \tag{11}$$

2.2 Wear coefficient α

The wear method described here requires an experimentally determined wear coefficient which encompasses a variety of parameters affecting wear such as material combination and properties, geometry, surface roughness, friction coefficient, lubrication regime, temperature, and loading frequency. In this study fretting wear is modelled in a commercial THR consisting of a cobalt chromium alloy femoral head and a titanium alloy stem. The fretting wear coefficient used $\alpha = 2.97\times10^{-8}$ MPa^{-1} was taken from Zhang, et al. [22] who used a pin on disk reciprocating sliding test for Co-28Cr-6Mo fretting on Ti-6Al-4V.

2.3 Wear fraction

The wear methodology can facilitate wearing of different head-stem material combinations whereby the proportion of wear that is removed from each of the contacting parts is specified by a 'wear fraction'. Simplistically, a wear fraction of (1:0) would remove all of the calculated wear from one part, whereas a wear fraction of (0.5:0.5) would remove the wear equally from both parts. As such, the wear depth removed from each part at the end of each analysis 'stage' is calculated as the product of the parts 'wear fraction' and the total wear depth determined for that particular 'stage'.

The wear fractions associated with the cobalt chrome 'head' and titanium 'stem' in this work have been specified as 0.9 for the Co-28Cr-6Mo and 0.1 for the Ti-6Al-4V following work by Bone, et al. [30] and

Langton, et al. [15]. The findings from their work indicate that the cobalt chrome head taper wears by around a factor of 10 more than the titanium alloy stem trunnion surface. This significant finding is supported further by work by Bishop, et al. [31] and has been explained by Moharrami, et al. [32] as occurring due to the preferential oxidation of titanium alloy over cobalt chrome thus increasing the hardness of the titanium trunnion which subsequently wears the un-oxidised CoCr head taper surface.

3. Finite Element Model

To predict wear accurately at the THR taper junction, the FE model used must be able to simulate the initial 'fixation' of the femoral head onto the stem trunnion in surgery, the subsequent weakening of this fixation, and the loading cycles to approximate hip loading during walking.

3.1 Geometry and mesh

The geometry of a commercial THR was used in the study to produce the FE model. The head and trunnion tapers were modelled with a zero taper mismatch angle (TMA) and meshed in preparation for analysis in ABAQUS 6.13-1 using eight-node bilinear hexahedral reduced integration elements (C3D8R) (see Fig. 3). Convergence studies were undertaken to ensure accurate and smooth evolution of wear at the taper interface with an element size of 0.2 mm being adequate in this respect.

3.2 Material properties, boundary conditions and interaction behaviour

The prosthesis components were modelled as deformable, linearly elastic with material properties as shown in Table 1.

Table 1
THR material properties

Material	Young's Modulus (GPa)	Poisson's ratio	Density (kg/m^3)
Co-28Cr-6Mo	210	0.3	7800
Ti-6Al-4V	119	0.29	4400

The loading applied on the model included an initial impact to simulate the assembly of the head onto the stem intra-operatively and then time variant loading cycles to approximate hip loading during walking.

The load-time history of the head-stem assembly impact event is shown in Fig. 4 with the maximum force set at 4000 N [1] (a value in the range typically applied by surgeons). During this impaction the base of the stem trunnion is fixed in all degrees-of-freedom.

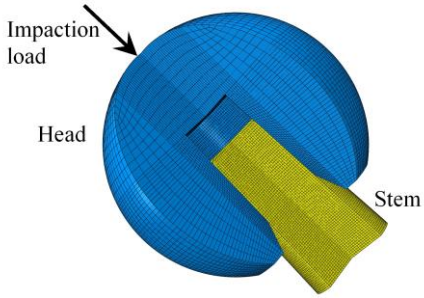

Fig. 3. FE model of the femoral head and stem trunnion of a commercial THR prosthesis.

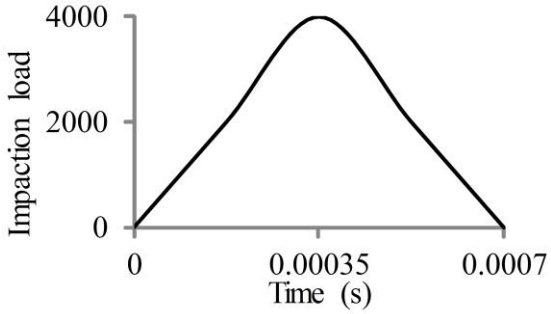

Fig. 4. The load history of the head-stem assembly (impact) event.

The loading and boundary conditions prescribed to the model during the walking cycle are shown in Fig. 5 [33] and include both time variant rotations and loadings about the three global coordinate directions. The rotations are applied to a point located at the centre of the head, this point being coupled to the proximal end of the stem trunnion. In addition, the outer head surface is coupled with a second point located at the centre of the head which has all of its translational degrees of freedom restrained but is allowed to rotate. This constrains the outer head surface so that it can only rotate about this centre point and therefore locates the head virtually in the acetabular cup. The hip forces were applied to the model via a third remote point (located virtually in the femur) coupled to the distal end of the truncated stem component providing realistic load transfer to the prosthetic components. These loads and boundary conditions provide a realistic and efficient model with no requirement to model acetabular cup and femoral bone. The hip load history was applied to the model with a peak force of 2000 N with the walking cycle discretised into 10 equal time intervals during the 1.2 s cycle time period. In this study an average of 1 million walking steps per year has been assumed based on the work by Schmalzried, et al. [34].

The contact interaction between the head and stem trunnion was modelled as ‘finite sliding’ using the ‘penalty’ contact formulation in ABAQUS and a constant isotropic coefficient of friction of 0.21 [35].

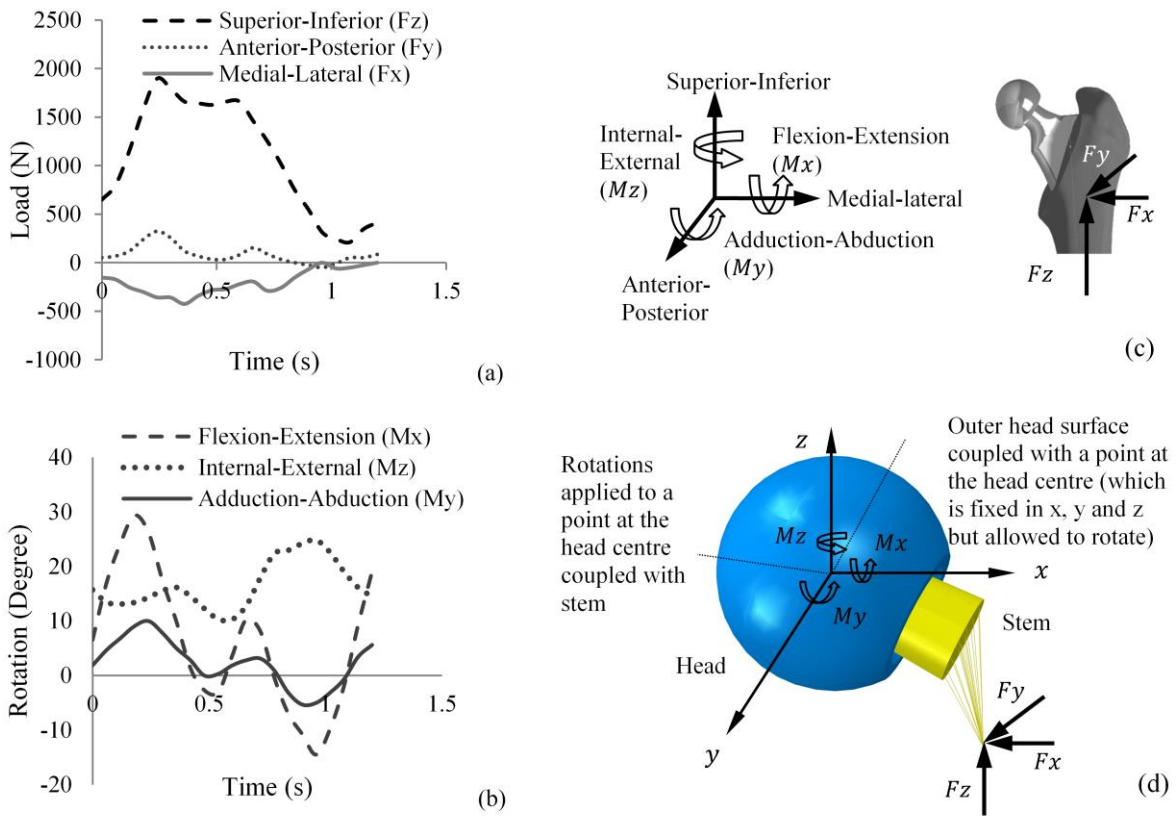

Fig. 5. Boundary conditions and loading, (a) hip loading, (b) hip rotation during a waling cycle, (c) load and rotational direction and (d) boundary condition and loads applied on 3D FE model.

4. Methodology

4.1 Algorithm and computational framework

The method presented here to predict wear contains three main phases which are necessary in order to accurately simulate the effect of impaction of the head onto the stem and the subsequent walking cycles.

In phase 1, the head and stem are assembled so that they just come into contact (no overlap). Then, a single dynamic implicit step is defined whereby the impaction load is applied to the top of the head to simulate the process of assembly of the head onto the stem in surgery. This analysis is only executed once so as to determine the necessary displacement of the parts to position the head into its assembled position relative to the stem trunnion for the commencement of phase 2 of the wear analysis method.

Prior to the commencement of phase 2 (which consists of two analysis steps) the parts are assembled based on the displacements obtained from phase 1 which creates overlap between the component meshes at the contact interface. Step 1 of phase 2 involves a ‘static contact analysis’ to re-simulate the ‘locking’ effect due to impaction (this is achieved by resolving the overlap). This static step is crucial in that it provides the mechanism to model the progressive weakening in the initial locking effect caused by fretting

wear at the taper interface (by subsequent removal of the overlap). In step 2 of phase 2, a dynamic implicit analysis is defined and the rotations and loading associated with a walking cycle (Fig. 5) are applied to the model. On completion of phase 2 (for a specific analysis 'stage' defined by β) the extent of fretting wear at the taper junction can be determined as a 'wear depth' at each set of paired nodes. Subsequently, the coordinates of these paired nodes are updated to reflect the wear that has occurred on each part during that analysis 'stage' with the wear depth removed from the taper surfaces in the normal direction of the contacting nodes. This updating partially removes the mesh overlap that is prevalent at the commencement of a 'stage' therefore gradually weakening the 'locking' effect created by impaction. The updating of the paired-nodes coordinates continues in this manner until the remaining overlap has been fully removed at which point the method continues into phase 3.

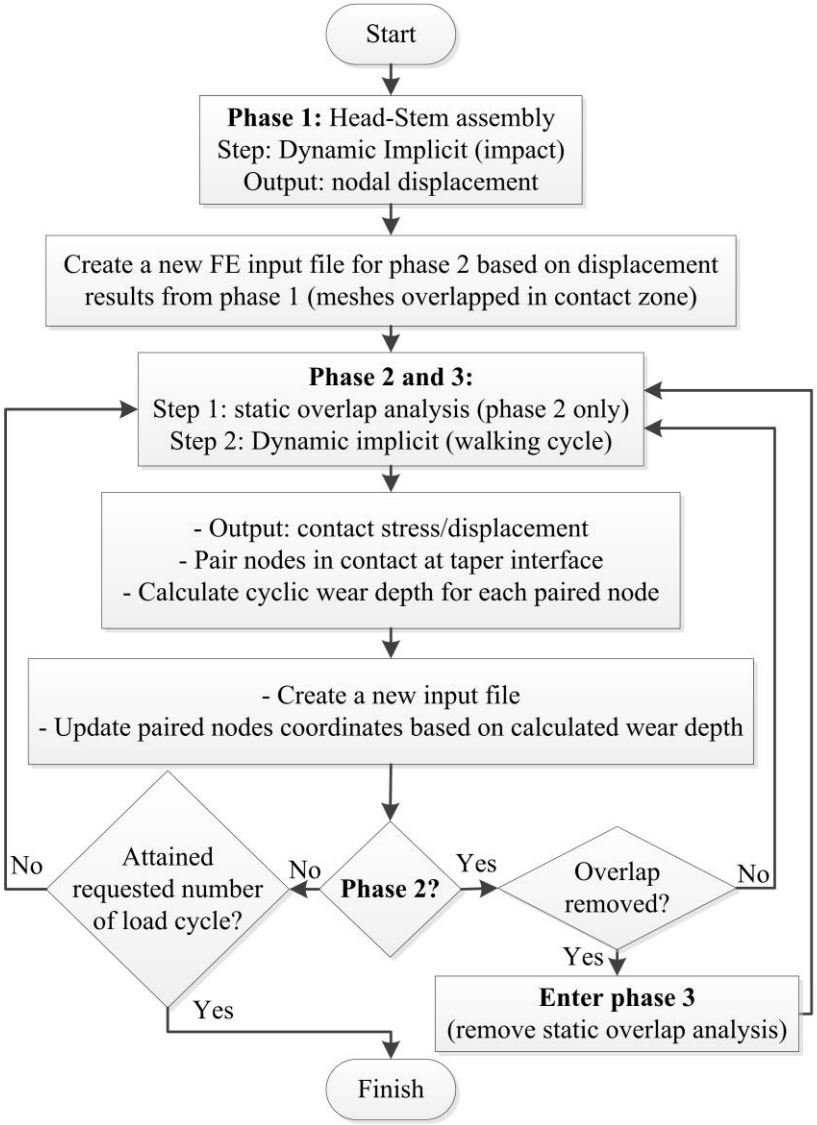

Fig. 6. Quantitative procedure to predict fretting wear.

In phase 3, as all of the overlap has now been removed, only a single dynamic implicit step (representing the hip walking cycle) is maintained for the rest of the analysis until the specified number of cycles or wear depth for the study has been reached. The method is illustrated in Fig. 6.

4.2 Automating the calculation of wear

Calculating wear for the paired nodes at the contact interface and updating their coordinate positions is a lengthy procedure. As such, the procedure for calculating the wear is automated in phase 2 and 3 using a Python script linked within ABAQUS as a user plug-in. The script initially submits the FE input file to ABAQUS then pairs nodes in the contact zone prior to application of hip loading. On completion of each time interval i the script extracts the contact shear stress and displacements for all of the paired nodes and then calculates the average shear stress τ_{ip} and relative displacement s_{ip} between them. Subsequently, the associated wear depth for each time interval is determined and then summed to provide a 'cyclic' wear depth which itself is then scaled by β to provide a sensible wear depth for updating purposes. Wear is then applied to the paired nodes (by updating their coordinate positions) in the opposite direction to their nodal normals in order to create new geometry for execution in the next analysis 'stage'. At the end of each analysis 'stage', the nodal wear depth calculated is written to the output database of ABAQUS for each contacting node in order to plot the wear depth pattern as the solution progresses.

5. Results and Discussion

A computational methodology has been presented to predict fretting wear at the taper interface between the head and stem of a THR. The uniqueness of the methodology is that it is able to simulate the progressive weakening of the initial head-stem fixation due to the wearing process. Simulating the reduction in the initial fixation strength of the head-stem assembly is seen as important to the accurate assessment of wear and has not been reported in the literature before. The following sections are presented to demonstrate and discuss key features and functionality of the methodology and the findings from the THR taper junction wear analysis.

Although an energy wear law is used in this study which is based on shear traction, the results which follow are illustrated based on contact pressure distribution for clarity. Contact shear stress has two components tangential to the contact surface and can be either positive or negative based on direction. As

such, shear stress distributions are difficult to interpret in the context of wear and so contact pressure has been presented instead.

5.1 FE mesh and wear scaling factor (β)

As with any finite element analysis model it is vital that a suitably refined mesh is generated in order to determine accurate results. It was found for this model that when there is a large variation in shear stress across individual elements in the contact zone (due to a too coarse mesh) vastly different wear depths for adjacent paired nodes will be calculated (as $W_d=\alpha\tau s$). This generates an uneven worn surface and can lead to future solution convergence problems and the calculation of an inaccurate wear depth (see Fig. 7). It is important that the mesh is highly refined in the contact zone so that variations in shear stress values across an individual element are kept to a minimum. To model the wearing process accurately and efficiently an element size of 0.2 mm (in the contact zone) was used in this study which allowed a smooth wear pattern to develop on the model as the solution progressed.

In addition, the scaling factor β used in the analysis has a major impact on solution times, wear evolution and solution accuracy too. This is demonstrated in Fig. 8 which shows the average wear depth that has occurred on the stem trunnion surface of the model after 2 million load cycles (2 years) when using scaling factors ranging from 50,000 to 2 million. A large scaling factor will facilitate a relatively quick analysis but may detrimentally affect the accuracy of the final calculated wear for a specified number of loading cycles. A comparatively small value for the scaling factor will increase solution times but should provide an accurate result and wear profile. A scaling factor of $\beta = 10^5$ was seen as necessary to produce the accuracy required for the wear depth (a scaling factor of 1 million developing around a 30% error, see Fig. 8). All analyses were executed with a scaling factor of 10^5 on a 64-bit Windows 7 professional operating system with twin dual six-core processor Intel Xeon central processing unit platforms at 2.60 GHz configured with 128 GB of random access memory. The time taken for each analysis ‘stage’ was on average around 6 hours, therefore, for an analysis of 5 million cycles (5 years), there would be 50 ‘stages’ summing to a total run-time of 300 hours.

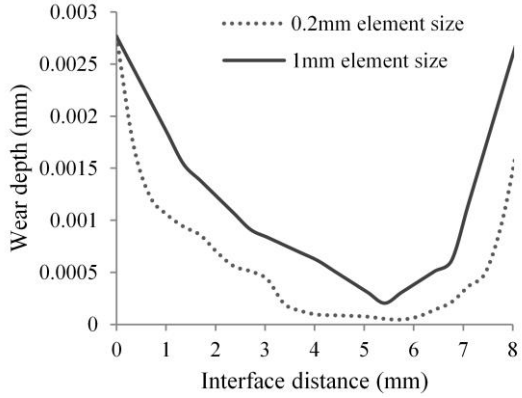

Fig. 7. Effect of element size on wear evolution (interface distance shown in Fig. 9).

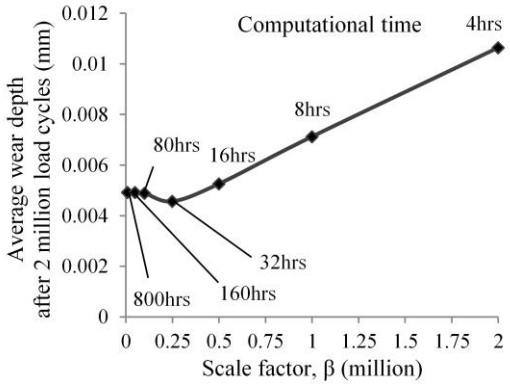

Fig. 8. Effect of different scaling factor values.

5.2 Initial assembly of prosthetic femoral head and stem

The initial fixation ('locking') of the femoral prosthetic head on the stem trunnion is generated by the surgeon impacting the head onto the stem intraoperatively. This is simulated here (in phase 1) by a single dynamic implicit analysis undertaken using the FE model shown in Fig. 3 and the load-time history shown in Fig. 4. It has been postulated that the initial fixation of the prosthetic head on the stem trunnion is reduced over time by fretting wear at their contacting surfaces. A key aspect of the wear methodology presented in this work is the use of an overlapped mesh at the taper interface with a static contact analysis step to model the weakening of this fixation (which is facilitated by the gradual removal of overlap with respect to time). As such, the contact conditions prevalent at the taper interface on completion of the dynamic analysis step (phase 1) need to be replicated at the start of step 2 in phase 2 by use of the static contact analysis step incorporating mesh overlap (step 1, phase 2).

The dynamic analysis undertaken in phase 1 provides part displacements that are used at the start of phase 2 to position the head and stem relative to one another so as to provide the necessary overlap for the static contact analysis step. Fig. 9 shows contact pressure distributions along the stem trunnion interface at the completion of phase 1 and at the commencement of step 2 in phase 2 (following the static contact analysis step). The figures show that the contact pressures computed from the dynamic (phase 1) and static contact (phase 2 step 1) analyses are almost identical and that use of a static contact analysis step (with overlap) can facilitate accurate modelling of the effect of impaction on head-stem fixation.

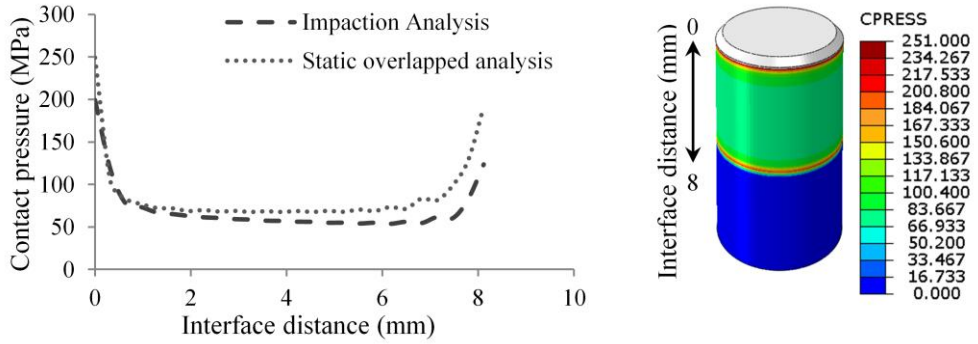

Fig. 9. Contact pressure distribution along stem trunnion surface at the end of phase 1 and at the commencement of step 2 of phase 2.

5.3 Variation in contact pressure and relative displacement during the walking cycle

The realistic gait cycle loading and rotation (Fig. 5 [33]) applied to the hip model generates varying contact pressure distributions, shear stress and relative displacements on the taper surface throughout its 1.2 s duration (see Fig. 10). As values for relative displacement and contact pressure will be equal and opposite on the head and stem taper surfaces, the change in relative displacement (or 'slip') is shown on Fig. 10 as distributed on the stem trunnion, whereas the variation in contact pressure is shown only on the head taper surface.

In Fig. 10 the distributions shown at time interval 0s are those determined from the initial static contact analysis (the contact conditions immediately after assembly of the head onto the stem). It can be seen that both the contact pressure and 'slip' distributions are symmetrical (as expected) and that maximum values occur at the edges of the taper contacts (both proximal and distal) with values of around 350 MPa and 9 μm. The majority of the taper surface is subject to a contact pressure of around 120 MPa, whereas the relative displacements are seen to reduce in magnitude from the taper edges to the taper central contact.

Fig. 5 indicates that the largest loading on the hip occurs in the 'superior-inferior' direction with the load increasing to its largest magnitudes between time intervals of 0.3 s and 0.7 s of the gait cycle (the same could 'loosely' be said about loading in the 'medial-lateral' and 'anterior-posterior' directions too).

Without considering the edge contacts, it can be seen that during the gait cycle the distribution of contact pressure changes, such that the largest pressures occur at the centre of the taper 'superior' surface (right hand side of taper plots), and the lowest values occur at the centre of the taper 'inferior' surface (left hand side). The maximum value for contact pressures occur between 0.3 s and 0.7 s (240 MPa at 0.72 s) in parallel with the applied loading. The relative displacements are seen to vary throughout the gait cycle

with the largest values due to edge contact (9 μm) occurring also during the time intervals when the loading is maximum (0.3 to 0.7 s) and reducing nearer to the end of the cycle. It can be observed that the micromotion values are very small as these distributions are those occurring immediately after impaction.

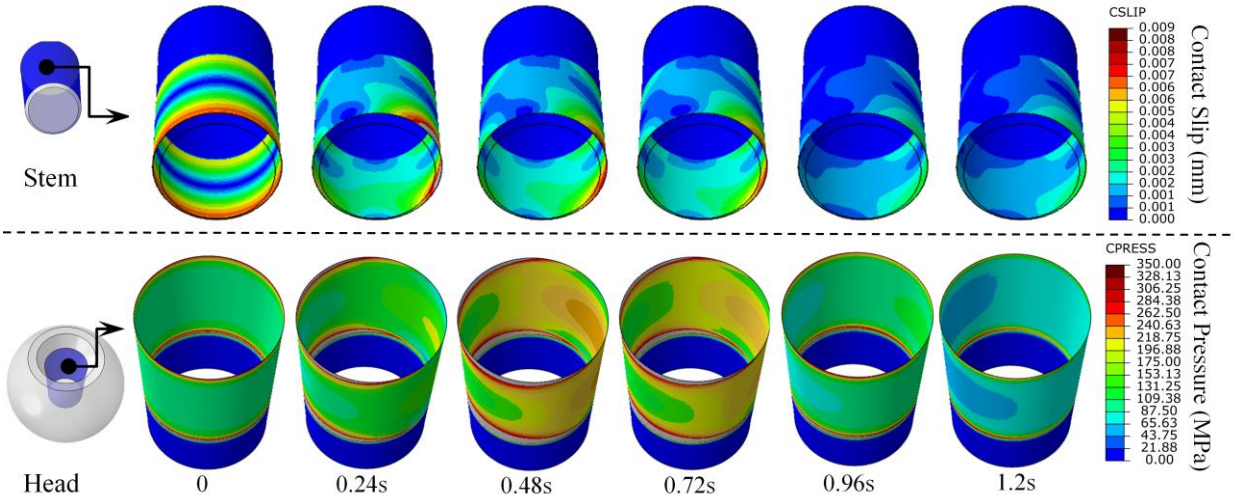

Fig. 10. Variation in contact pressure and relative displacement during a walking cycle.

5.4 Variation in taper wear over 5 year period

Fig. 11 shows the variation of contact pressure and relative displacement as well as the evolution of taper wear over a five year period of time. During the first 2.6 million cycles of loading it can be seen that the contact pressure generally reduces from the initial uniform distribution of 120 MPa following assembly (Fig. 10) to a non-uniform distribution with the majority of the taper surface subject to contact pressure values of around 30 MPa at the last time interval (Fig. 11c). Conversely, the 'bulk' values of taper relative displacement ('slip') are seen to increase during the same time period from a value of around 2 μm (Fig. 10) at assembly to around 38 μm at 2.6 million cycles (Fig. 11b). This reduction in contact pressure and increase in 'slip' is due to the gradual weakening of the taper fixation (modelled by a reduction in mesh overlap due to wear) with respect to time. At 2.6 million cycles the initial overlap has been completely removed and the analysis moves from phase 2 to phase 3 of the methodology.

During the loading period 3 to 5 million cycles the contact pressure distribution remains relatively constant with only a small reduction in contact pressure. During the same time period the relative displacements continue to increase on the inferior taper surface (left side) with values approaching 100 μm in localised areas; on the superior taper surface (right side) the values of 'slip' tended to decrease with localised areas indicating values of between 0 and 30 μm. The greater relative increase in 'slip' with minimal change to contact pressure in phase 3 creates an increase in wear rate in localised areas.

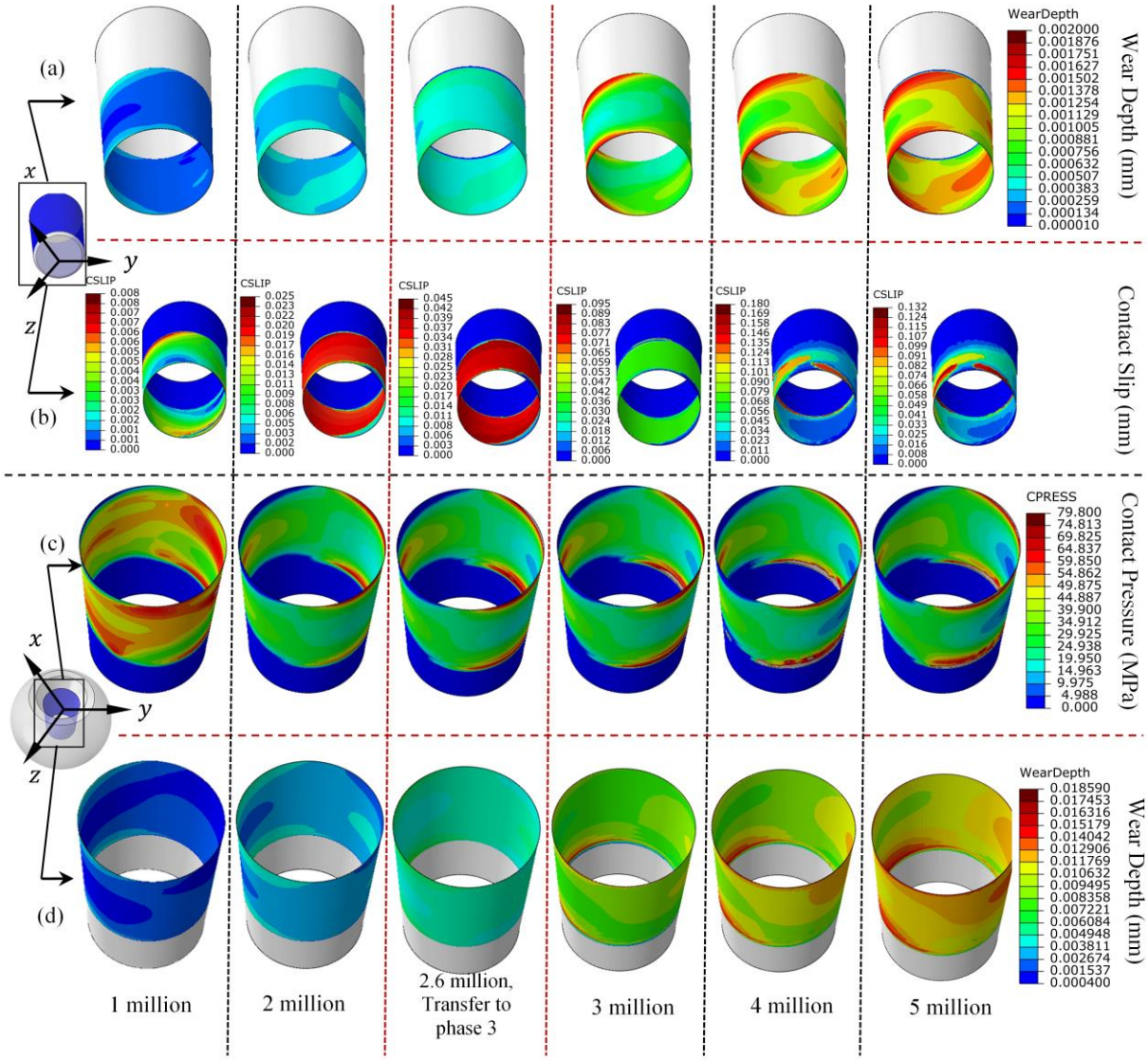

Fig. 11. Evolution of contact pressure, slip and wear pattern during wear analysis, row (a) and (b) show the pattern of wear depth in mm and contact slip changes on the stem trunnion, row (c) and (d) show the contact pressure in MPa and the pattern of wear depth in mm on the head taper, results shown at the last time interval.

It can be seen from Fig. 11 that the wear depth on the titanium stem trunnion (Fig. 11a) and in the cobalt chrome head taper (Fig. 11d) at 5 million cycles are different by a factor of around 10 (as dictated by the 'wear fractions' associated with each part) at 2 μm and 18.6 μm respectively on the inferior surface taper edges (left hand side of plots). It is necessary in the wear analysis of metal head-stem taper junctions (and for MoM prostheses) to update the contact surface geometry of both parts of the prosthesis as this has an effect on the wear rate and wear pattern following each analysis 'stage'. The wear pattern develops from a uniform zero wear pattern at the outset of the study to a non-uniform pattern with maximum wear occurring at the taper edges and on the superior surface of the taper, and minimum wear on the inferior surface at 5 million cycles (5 years).

5.5 Volumetric wear rate

The volumetric wear rate was determined based on the reduction of element volume for all elements in the contact zone. The volumetric wear rate was calculated following each 1 million cycles as the solution progressed (Fig. 12). It can be seen that the lowest wear rates occurred during the first 2 years (2 million cycles) with total values of 0.4 and 0.36 mm^3/yr. Subsequently it can be seen that the wear rate increases to a value of 0.66 mm^3/yr at 4 years. This is around a 50% increase in the wear rate and can be attributed to the removal of the initial taper locking effect and the subsequent increase in relative displacement at around 2.6 million cycles. The increase in wear rate can be linked to a 'transition' point whereby the initial locking effect of the head-stem taper has been fully removed and increased micromotion occurs resulting in an increase in wear rate.

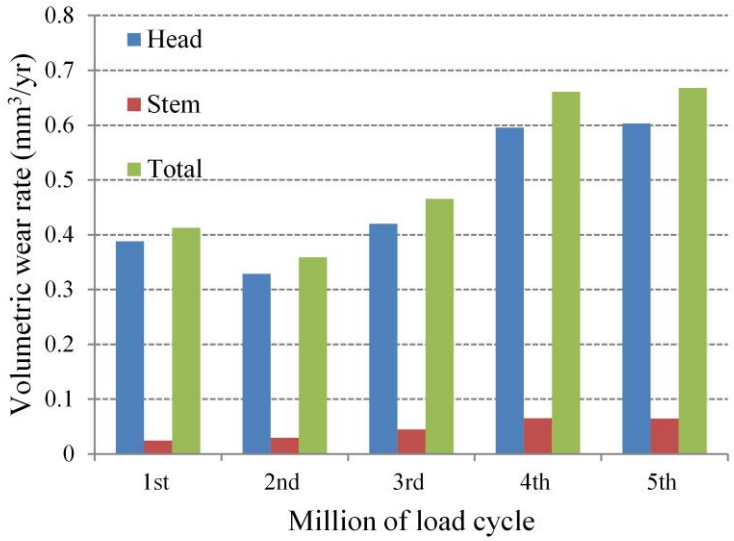

Fig. 12. Variation in volumetric wear rate with respect to time.

Table 2 details the average linear and volumetric wear rates over the 5 year period of study. The wear rates for the head were 1.917 μm/yr and 0.467 mm^3/yr, whereas the stem wear rates were 0.213 μm/yr and 0.0459 mm^3/yr.

Table 2
Average linear and volumetric wear rate on head taper and stem trunion

	Head (Co-Cr)	Stem (Ti)	Total
Wear fraction	0.9	0.1	1
Average linear wear rate (μm/yr) (range)	1.917 (0.8 – 18.5)	0.213 (0.01-0.4)	N/A
Average volumetric wear rate (mm^3/yr) (range)	0.467 (0.329 – 0.603)	0.0459 (0.024 -0.065)	0.513

5.6 Validation

The results for taper wear (Fig. 11) determined from the numerical wear analysis can be compared favourably with images and measurements from retrieved prostheses (retrieval prior to 5 years service). Fig. 13 shows a comparison of the wear patterns associated with the numerical analysis and images of wear occurring on the head taper of a retrieved Birmingham XL femoral head. Several retrieved prostheses were available for inspection, all of which demonstrated similar wear damage as that shown in Fig. 13. It can be seen in Fig. 11that the wear pattern at any stage of phase 3 of the numerical analysis tends to be fairly constant and can be effectively compared against the wear observed in retrieved prostheses where common wear patterns tend to prevail too (as walking is overwhelmingly the most common activity in patients with a hip implant). Observation of Fig. 13 shows that the extent of wear damage and patterns on the FE model are similar to the areas of wear shown on the images of the retrieved prosthesis. The wear damage seen on the surface of the retrieved prosthesis has been categorised as severe, moderate and minor. In the areas of severe wear it is likely that initial adhesive wear due to fretting has developed into abrasive wear due to retained wear particles which have subsequently promoted corrosion. In the areas shown as having moderate damage it is possible that any wear particles have been able to exit the contact zone so exhibiting a less damaged surface likely generated by adhesive wear and corrosion. The smooth surface highlighted as minor wear will be the result of adhesive wear only. It can be seen that the wear algorithm has identified accurately the areas of severe, moderate and minor wear damage based purely on the assumption of mechanical fretting wear. This is to be expected as any corrosion occurring on the taper surface will be due to mechanically assisted crevice corrosion (MACC) whereby fretting wear continually disrupts the protective surface oxide passivation layer of the taper junction materials exposing the metal and making it more susceptible to corrosion.

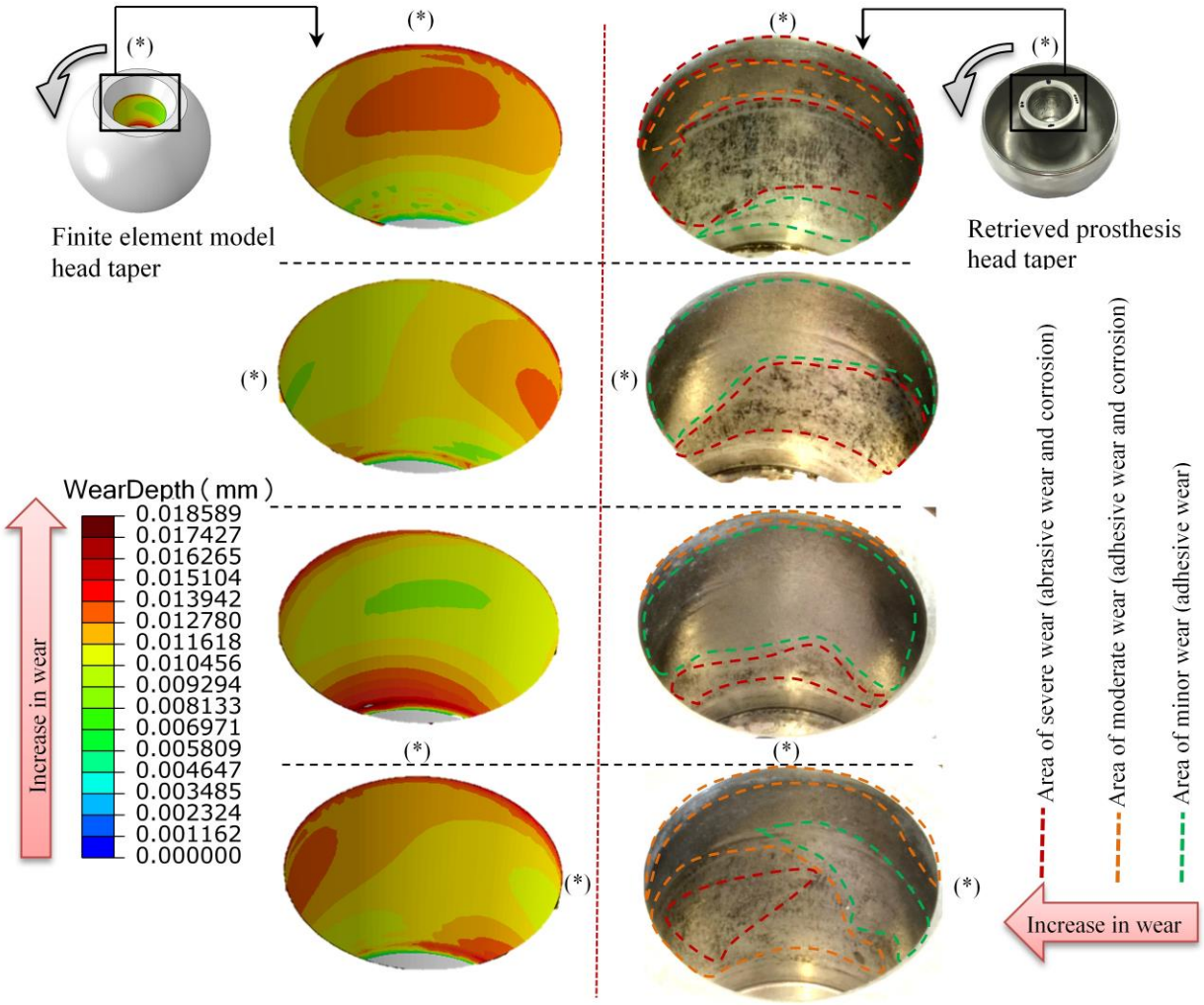

Fig. 13. Validation against retrieved prostheses. Figures are rotated anticlockwise based on label shown as (*).

In addition to these observations, the wear pattern and wear rates determined in these studies are similar to those obtained by Langton, et al. [15] for measurements obtained for retrieved Articular Surface Replacement XL THRs (ASR; DePuy, Leeds, United Kingdom). Langton, et al. [15] used a highly accurate CMM (accuracy 0.8 µm) to measure linear and volumetric wear occurring at the head taper surface of retrieved large diameter MOM THRs (Articuleze (48 components) and ASR XL (63 components), Depuy). The median time *in vivo* for the Articuleze and ASR XL prostheses was approximately 1 to 5 years respectively with the mean volumetric wear rate for Articuleze being 0.127 mm^3/yr (range 0.01-3.15) and the ASR XL measured at 0.44 mm^3/yr (range 0.02-8.34). The small differences in volumetric wear rate determined in this study (see Table 2) in comparison to Langton can be attributed to differences in the head-stem material combinations, wear coefficient, material loss due to corrosion and THR design. In addition, the effect of initial assembly of the head and stem is unclear and

could be one of the reasons for the slight differences in wear rates too. Malviya, et al. [17] also used the same CMM as Langton, et al. [15] and presented the wear pattern on the 2-year follow up of a retrieved Birmingham hip replacement . The investigation showed no material loss or corrosion on the articular bearing surfaces, but a wear depth of 6 μm on the head taper. The wear pattern shown in Fig. 11 at 2 million load cycles (2 years) on the head taper is within the same range of wear depth.

The close similarities shown between the numerical analysis and the observed and measured wear damage of retrieved prostheses demonstrates the effectiveness of the 3D FE model, loading, boundary conditions and wear algorithm used.

6. Conclusions

A computational methodology and 3D FE model has been presented which can be used to accurately predict the extent of fretting wear which can occur at the taper junction between the head and stem of a modular THR during its expected operational lifetime. The method could be used in design or applied to clinical practice to help facilitate a reduction in wear.

The methodology demonstrates that a static contact analysis incorporating mesh overlap can effectively model taper fixation (created during assembly of head and stem in surgery) and also the progressive weakening of this fixation due to the wearing process. This is achieved by removing overlap in line with calculated wear as the solution progresses and is seen as a novel aspect of the wear method described.

The total dissipated energy wear law and the FE model described can predict linear wear depth and damage patterns effectively when compared to typical observed wear patterns and measured wear depths from retrieved prostheses. The comparisons undertaken show considerable promise but are clearly dependent on the use of an appropriate wear coefficient and knowledge of the retrieved prostheses loading history. Accurate determination of wear of individual THR components can be realised by measurement from retrieved prostheses or from fretting wear tests. These measurements can then provide accurate wear fractions for application in computational wear analysis. In addition, it should be noted that the wear coefficient α is related to the component pair in contact and is used in the calculation of total wear, it does not differentiate as to the extent of wear occurring on each surface, as such, the use of component ‘wear fractions’ is required.

The accurate and smooth evolution of wear across the contact interface has been demonstrated with the guideline to incorporate a highly refined mesh in the contact zone to avoid local ‘spikes’ in the contact stresses due to a too large element size. Further, the wear scaling factor used in the analysis has a major effect on simulation run times and can affect the accuracy of the analysis results and the evolution of wear. A too large scaling factor can create an uneven wear profile across the contact interface due to cyclic wear “hot spots” being overtly increased. In contrast, a comparatively small scaling factor will facilitate an accurate and smooth development of wear but with the cost of a much increased run time. In this specific application, a scaling factor of 0.1 million was appropriate.

Limitations of the method can be considered as being the significance that the energy wear coefficient has on the resulting wear depth and the simplifying boundary conditions used in the study. The boundary conditions used (although creating an efficient model by excluding the requirement to model the acetabular cup), create non-physiologic resisting moments at the centre of the head which need to be acknowledged when interpreting any results from an analysis. Further, the boundary conditions provide a restriction to the analysis of certain design / operational considerations which may be related to fretting wear such as head size and frictional torque. The analysis of these aspects of prosthesis design will require a modified model to that described here which by necessity will require the inclusion of the acetabular cup and an additional contact region thus increasing computational effort considerably. These limitations are currently been addressed by the authors.

The wear methodology can be utilized generically in the analysis of other prosthetic devices such as knee and shoulder modular implants. In addition, the method could be generalized to predict fretting wear for any components which involve parts in contact subject to oscillatory loads and micromotion.

Acknowledgment

This work is funded by the School of Engineering, Technology and Maritime Operations, Liverpool John Moores University, Liverpool, UK. The authors would like to acknowledge Mr Viju Peter, Mr Alasdair Santini and Mr Andrew Phillipson, orthopaedic surgeons from Broadgreen Hospital, Liverpool, UK, for their advice and cooperation. We would also like to acknowledge Professor Thomas Joyce from Newcastle University, Newcastle, UK for his advice.

References

[1] J. P. Heiney, S. Battula, G. A. Vrabec, A. Parikh, R. Blice, A. J. Schoenfeld, *et al.*, "Impact magnitudes applied by surgeons and their importance when applying the femoral head onto the Morse taper for total hip arthroplasty," *Archives of Orthopaedic and Trauma Surgery*, vol. 129, pp. 793-796, 2009.

[2] D. Langton, S. Jameson, T. Joyce, J. Gandhi, R. Sidaginamale, P. Mereddy, *et al.*, "Accelerating failure rate of the ASR total hip replacement," *Journal of Bone & Joint Surgery, British Volume*, vol. 93, pp. 1011-1016, 2011.

[3] L. Mattei, F. Di Puccio, B. Piccigallo, and E. Ciulli, "Lubrication and wear modelling of artificial hip joints: A review," *Tribology International*, vol. 44, pp. 532-549, 2011.

[4] J. C. Fialho, P. R. Fernandes, L. Ecca, and J. Folgado, "Computational hip joint simulator for wear and heat generation," *Journal of Biomechanics*, vol. 40, pp. 2358-2366, 2007.

[5] T. A. Maxian, T. D. Brown, D. R. Pedersen, and J. J. Callaghan, "3-Dimensional sliding/contact computational simulation of total hip wear," *Clinical Orthopaedics and Related Research*, vol. 333, pp. 41-50, 1996.

[6] T. A. Maxian, T. D. Brown, D. R. Pedersen, and J. J. Callaghan, "A sliding-distance-coupled finite element formulation for polyethylene wear in total hip arthroplasty," *Journal of Biomechanics*, vol. 29, pp. 687-692, 1996.

[7] T. A. Maxian, T. D. Brown, D. R. Pedersen, H. A. McKellop, B. Lu, and J. J. Callaghan, "Finite element analysis of acetabular wear: validation, and backing and fixation effects," *Clinical Orthopaedics and Related Research*, vol. 344, pp. 111-117, 1997.

[8] S. Patil, A. Bergula, P. C. Chen, C. W. ColwellJr, and D. D. D'Lima, "Polyethylene wear and acetabular component orientation," *The Journal of Bone & Joint Surgery*, vol. 85, pp. 56-63, 2003.

[9] M. Raimondi, C. Santambrogio, R. Pietrabissa, F. Raffelini, and L. Molfetta, "Improved mathematical model of the wear of the cup articular surface in hip joint prostheses and comparison with retrieved components," *Proceedings of the Institution of Mechanical Engineers, Part H: Journal of Engineering in Medicine*, vol. 215, pp. 377-390, 2001.

[10] S. Teoh, W. Chan, and R. Thampuran, "An elasto-plastic finite element model for polyethylene wear in total hip arthroplasty," *Journal of Biomechanics*, vol. 35, pp. 323-330, 2002.

[11] J. S. S. Wu, J. P. Hung, C. S. Shu, and J. H. Chen, "The computer simulation of wear behavior appearing in total hip prosthesis," *Computer Methods and Programs in Biomedicine*, vol. 70, pp. 81-91, 2003.

[12] D. Cohen, "How safe are metal-on-metal hip implants?," *BMJ: British Medical Journal*, vol. 344, 2012.

[13] S. M. Sporer and P. N. Chalmers, "Cutaneous manifestation of metallosis in a Metal-on-Metal total hip arthroplasty after acetabular liner dissociation," *The Journal of Arthroplasty*, vol. 27, pp. 1580-e13, 2012.

[14] X. Mao, G. H. Tay, D. B. Godbolt, and R. W. Crawford, "Pseudotumor in a well-fixed metal-on-polyethylene uncemented hip arthroplasty," *The Journal of Arthroplasty*, vol. 27, pp. 493-e13, 2012.

[15] D. Langton, R. Sidaginamale, J. Lord, A. Nargol, and T. Joyce, "Taper junction failure in large-diameter metal-on-metal bearings," *Bone and Joint Research*, vol. 1, pp. 56-63, 2012.

[16] B. Bolland, D. Culliford, D. Langton, J. Millington, N. Arden, and J. Latham, "High failure rates with a large-diameter hybrid metal-on-metal total hip replacement " *Journal of Bone & Joint Surgery, British Volume*, vol. 93, pp. 608-615, 2011.

[17] A. Malviya, J. Ramaskandhan, R. Bowman, M. Hashmi, J. Holland, S. Kometa, *et al.*, "What advantage is there to be gained using large modular metal-on-metal bearings in routine primary hip replacement? A preliminary report of a prospective randomised controlled trial," *Journal of Bone & Joint Surgery, British Volume,* vol. 93, pp. 1602-1609, 2011.

[18] J. R. Goldberg, J. L. Gilbert, J. J. Jacobs, T. W. Bauer, W. Paprosky, and S. Leurgans, "A multicenter retrieval study of the taper interfaces of modular hip prostheses," *Clinical Orthopaedics and Related Research,* vol. 401, pp. 149-161, 2002.

[19] J. L. Gilbert, C. A. Buckley, and J. J. Jacobs, "In vivo corrosion of modular hip prosthesis components in mixed and similar metal combinations. The effect of crevice, stress, motion, and alloy coupling," *Journal of Biomedical Materials Research,* vol. 27, pp. 1533-1544, 1993.

[20] N. J. Hallab, C. Messina, A. Skipor, and J. J. Jacobs, "Differences in the fretting corrosion of metal–metal and ceramic–metal modular junctions of total hip replacements," *Journal of Orthopaedic Research,* vol. 22, pp. 250-259, 2004.

[21] L. Duisabeau, P. Combrade, and B. Forest, "Environmental effect on fretting of metallic materials for orthopaedic implants," *Wear,* vol. 256, pp. 805-816, 2004.

[22] T. Zhang, N. Harrison, P. McDonnell, P. McHugh, and S. Leen, "A finite element methodology for wear-fatigue analysis for modular hip implants," *Tribology International,* vol. 65, pp. 113-127, 2013.

[23] J. M. Elkins, J. J. Callaghan, and T. D. Brown, "Stability and Trunnion Wear Potential in Large-diameter Metal-on-Metal Total Hips: A Finite Element Analysis," *Clinical Orthopaedics and Related Research,* vol. 472, pp. 529-542, 2014.

[24] J. M. Elkins, M. K. O'Brien, N. J. Stroud, D. R. Pedersen, J. J. Callaghan, and T. D. Brown, "Hard-on-hard total hip impingement causes extreme contact stress concentrations," *Clinical Orthopaedics and Related Research,* vol. 469, pp. 454-463, 2011.

[25] F. Liu, I. Leslie, S. Williams, J. Fisher, and Z. Jin, "Development of computational wear simulation of metal-on-metal hip resurfacing replacements," *Journal of Biomechanics,* vol. 41, pp. 686-694, 2008.

[26] M. Uddin and L. Zhang, "Predicting the wear of hard-on-hard hip joint prostheses," *Wear,* vol. 301, pp. 192-200, 2013.

[27] S. Fouvry, T. Liskiewicz, P. Kapsa, S. Hannel, and E. Sauger, "An energy description of wear mechanisms and its applications to oscillating sliding contacts," *Wear,* vol. 255, pp. 287-298, 2003.

[28] R. Magaziner, V. Jain, and S. Mall, "Wear characterization of Ti–6Al–4V under fretting–reciprocating sliding conditions," *Wear,* vol. 264, pp. 1002-1014, 2008.

[29] T. Liskiewicz and S. Fouvry, "Development of a friction energy capacity approach to predict the surface coating endurance under complex oscillating sliding conditions," *Tribology international,* vol. 38, pp. 69-79, 2005.

[30] M. C. Bone, R. P. Sidaginamale, J. K. Lord, S. C. Scholes, T. J. Joyce, A. V. Nargol, *et al.*, "Determining material loss from the femoral stem trunnion in hip arthroplasty using a coordinate measuring machine," *Proceedings of the Institution of Mechanical Engineers, Part H: Journal of Engineering in Medicine,* vol. 229, pp. 69-76, 2015.

[31] N. Bishop, F. Witt, R. Pourzal, A. Fischer, M. Rütschi, M. Michel, *et al.*, "Wear patterns of taper connections in retrieved large diameter metal-on-metal bearings," *Journal of Orthopaedic Research,* vol. 31, pp. 1116-1122, 2013.

[32] N. Moharrami, D. Langton, O. Sayginer, and S. Bull, "Why does titanium alloy wear cobalt chrome alloy despite lower bulk hardness: A nanoindentation study?," *Thin Solid Films,* vol. 549, pp. 79-86, 2013.

[33] G. Bergmann, F. Graichen, and A. Rohlmann, "Hip joint loading during walking and running, measured in two patients," *Journal of Biomechanics,* vol. 26, pp. 969-990, 1993.

[34] T. P. Schmalzried, E. S. Szuszczewicz, M. R. Northfield, K. H. Akizuki, R. E. Frankel, G. Belcher, *et al.*, "Quantitative Assessment of Walking Activity after Total Hip or Knee Replacement*," *The Journal of Bone & Joint Surgery*, vol. 80, pp. 54-9, 1998.

[35] H. Fessler and D. Fricker, "Friction in femoral prosthesis and photoelastic model cone taper joints," *Proceedings of the Institution of Mechanical Engineers, Part H: Journal of Engineering in Medicine*, vol. 203, pp. 1-14, 1989.